Improved Geolocation and Earth Incidence Angle Information for a Fundamental Climate Data Record of the SSM/I Sensors

Wesley Berg, Mathew R. P. Sapiano, Jennifer Horsman, and Christian Kummerow

***Abstract*—The long-term data record of microwave imager data from the series of six Special Sensor Microwave/Imagers (SSM/Is) on board the Defense Meteorological Satellite Program (DMSP) spacecraft has been used to produce global multidecadal time series of a number of geophysical parameters, including precipitation, total precipitable water, ocean surface wind speed, and sea ice extent. As part of an effort to produce an intercalibrated fundamental climate data record (CDR) of the brightness temperature (Tb) data from the SSM/I, an examination of geolocation errors and the subsequent impact on the view angle [or the Earth incidence angle (EIA)] is performed. Using a combination of techniques, estimates of changes in the sensor/spacecraft attitude, including deviations in roll, pitch, and yaw, have been computed for the life of each of the SSM/I sensors. Applying these corrections results in an improved pixel geolocation, but more importantly, it provides accurate estimates of the EIA across the scan and throughout each orbit. An analysis of uncertainties in the calculation of EIA shows mean errors within 0.1°, which translates to errors in the calibration of less than 0.2 K for all channels. The availability of these precise estimates of EIA is extremely important for producing CDRs since the mean EIA decreases over time due to the decay in the DMSP orbits, which will lead to an artificial climate trend if not properly accounted for by the geophysical retrieval algorithms.**

***Index Terms*—Calibration, geolocation, microwave radiometry, satellites.**

I. Introduction

PASSIVE microwave imager data from satellites have provided over two decades of nearly continuous global observations of geophysical parameters that are used to monitor the climate system. This includes such fields as precipitation over both land and ocean, total precipitable water (TPW), cloud liquid water, surface wind speed over oceans, soil moisture and snow cover over land, and ice extent and sea ice concentration over polar regions. Since June 1987, six Special Sensor Microwave/Imager (SSM/I) window-channel radiometers have been launched on board the Defense Meteorological Satellite Program's (DMSP) series, including the F08, F10, F11, F13, F14, and F15 spacecraft [1], [2]. As a result, this data record provides the best available source of long-term global observations for many of the geophysical parameters listed earlier.

Creating a consistent long-term climate data record (CDR) of geophysical retrieval or a thematic CDR (TCDR) requires that the input data, in this case the brightness temperature (Tb), be physically consistent over the life of each sensor as well as between sensors. An intercalibrated Tb data set such as this is referred to as a fundamental CDR (FCDR), which has been defined by the National Research Council as "sensor data (e.g., calibrated radiance, Tb, and radar backscatter) that have been improved and quality controlled over time, together with the ancillary data used to calibrate them" [3]. Although the DMSP sensors provide a long-term record, they were developed for operational applications such as numerical weather prediction. For most climate applications using these data, long-term stability and consistency within 0.5 K or better are required. As such, issues such as view-angle changes associated with spacecraft altitude variations and orbit decay, the impact of sensor heating due to changes in Earth shadowing, and other factors affecting the overall calibration and/or changes in calibration must be addressed in order to produce a consistent data set suitable for use in climate applications. While a number of techniques have been developed to intercalibrate the SSM/I sensors [4]–[8], for the most part, these approaches have assumed that the SSM/I sensors are identical or, at least, similar enough to effectively ignore the impact of sensor differences. As a result, most intercalibration work has focused directly on intercomparing the observed Tb from sensors with overlapping data records.

The six SSM/I sensors were built as identical copies of each other with the same channel complement and scan geometry, and each of the instruments was mounted to the spacecraft bus at a nominal angle of 45°. Slight differences in the mount angle due to tolerances, small deviations in the attitude of the spacecraft, and errors in the calculated position of the spacecraft, however, result in errors in the pixel geolocation [2], [9]. With F08, Poe and Conway [9] found geolocation errors on the order of 20–30 km, which were subsequently reduced to 10–12 km using an improved spacecraft ephemeris. To further reduce the geolocation errors below ∼5 km, they calculated and applied a fixed set of spacecraft attitude corrections. Since all of the

Manuscript received January 19, 2012; revised April 4, 2012; accepted May 10, 2012. Date of publication July 13, 2012; date of current version February 21, 2013. This work was supported by the National Oceanic and Atmospheric Administration under Grant NA09OAR4320893#9.

W. Berg and C. Kummerow are with the Department of Atmospheric Science, Colorado State University, Fort Collins, Colorado 80523 USA (e-mail: berg@atmos.colostate.edu).

M. R. P. Sapiano is with the Earth Systems Science Interdisciplinary Center, University of Maryland, College Park, MD 20742 USA.

J. Horsman is with the Visualization Group, Lawrence Berkeley National Laboratory, Berkeley, CA 94720 USA.

Color versions of one or more of the figures in this paper are available online at http://ieeexplore.ieee.org.

Digital Object Identifier 10.1109/TGRS.2012.2199761

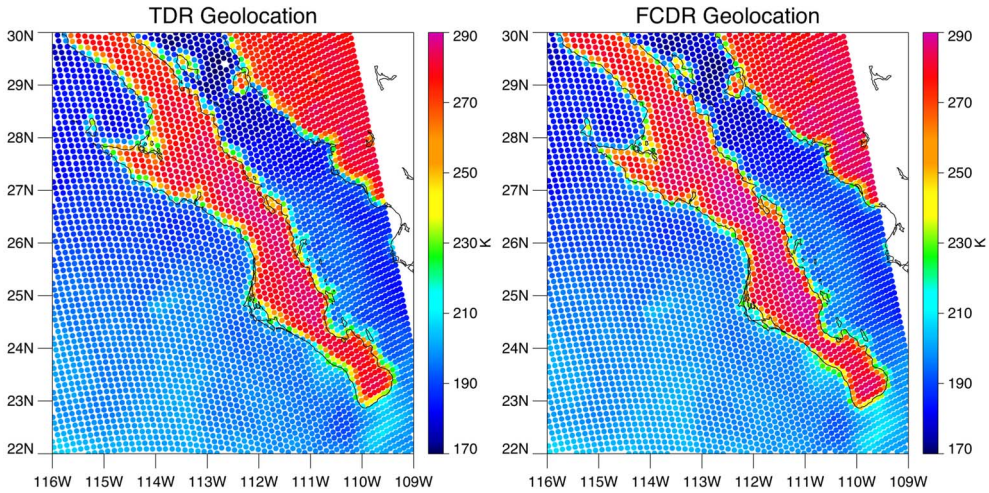

Fig. 1. Image of the full-resolution 85-GHz horizontally polarized Tb pixel data using (a) original TDR pixel geolocation and (b) final FCDR geolocation, which has the spacecraft attitude offsets applied. The image shown corresponds to the ascending orbit pass from F13 taken on May 2, 1996, over the Gulf of California.

SSM/I channels are window channels, any geolocation errors are apparent between the coastal outline evident in the observed Tb, as shown in Fig. 1(a). Although this shift is small relative to the spatial resolution of the sensor, a close examination shows an eastward shift in the Tb relative to the coastline overlay. This shift is subsequently removed in the final FCDR geolocation shown in Fig. 1(b) after the application of roll, pitch, and yaw offsets.

While the direct consequence of geolocation errors on the order of 10–12 km is minimal for most applications, pixel geolocation errors can be caused by offsets in the spacecraft attitude, which in turn impact the view angle or the Earth incidence angle (EIA) [9]. Small differences in the EIA can have a significant impact on the observed Tb, which, if not accounted for, can impact the intercalibration as well as subsequent geophysical retrieval. Using information on the spacecraft altitude from the calculated ephemeris along with attitude offsets, which were computed from the subsequent geolocation analysis, EIA estimates have been computed for each pixel. Fig. 2 shows the changes in the EIA across the scan and over the orbit, which are due to variations in the altitude and attitude of the spacecraft. In this case, the EIA varies by more than 0.5° across the orbit, which is typical. If two SSM/I sensors view the same scene with a slightly different view angle, the sensor with the larger or more acute angle will view more atmosphere along the slant path. In addition, over water, the surface emissivity is a function of the view angle and polarization, which tends to mostly cancel the atmospheric effect for horizontally polarized channels but enhances the difference in observed Tb for vertically polarized channels.

Fig. 3 shows the difference between simulated Tb over tropical and subtropical oceans from F13 using a fixed nominal EIA of 52.94, as determined by Colton and Poe [2], versus using a calculated EIA, which accounts for variations in altitude across the orbit but not for attitude offsets. It should be noted that the nominal EIA includes the impact of an elevation offset in the sensor alignment of 0.05° and a fixed on-orbit pitch offset of −0.3°. The simulated Tb are computed using an optimal estimation (OE) approach developed in [10] to retrieve

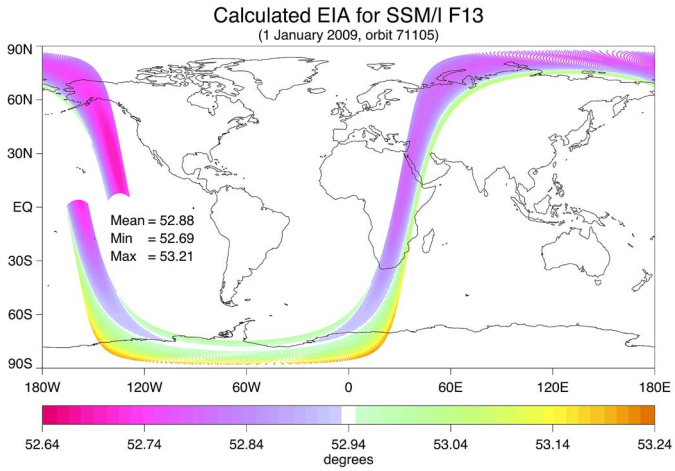

Fig. 2. Plot of the calculated EIA for a single orbit of SSM/I F13. The color scale shows deviations from the nominal value of 52.94 calculated in [2].

atmospheric and ocean surface parameters from the observed Tb. The retrieved parameters are then used as input into a radiative transfer model to compute simulated Tb using the two different EIA assumptions. The use of model analyses from the European Centre for Medium-Range Weather Forecasts to obtain the atmospheric and ocean surface parameters instead of the OE gives very similar results. The procedure for calculating the EIA, as well as the pixel geolocation, is discussed in the following section. As shown in Fig. 3, for the horizontally polarized channels, the difference in Tb is relatively small with values between 0.2 and −0.2 K, although it is not insignificant. For the vertically polarized channels, the impact is significantly larger with differences varying from −0.2 to −0.7 K. In addition, the Tb difference is a function of the scene temperature for all of the channels. The implication of this is that expected differences in the observed Tb due to differences in the EIA between two sensors must be properly accounted for, or as shown in Fig. 3, significant errors could result in the intercalibration of the sensors depending on both the channel and scene temperature.

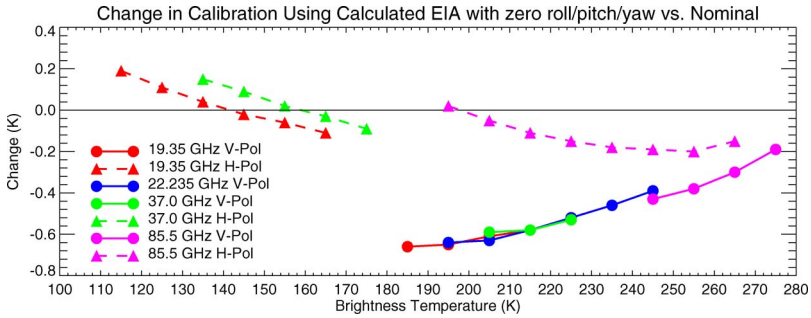

Fig. 3. Simulated differences in F13 Tb during 2008 based on the nominal EIA versus the altitude varying EIA. The nominal EIA of 52.94 was obtained in [2], whereas the calculated EIA values are based on the spacecraft position calculated using TLE data and assuming no mount angle errors as well as zero roll, pitch, and yaw offsets.

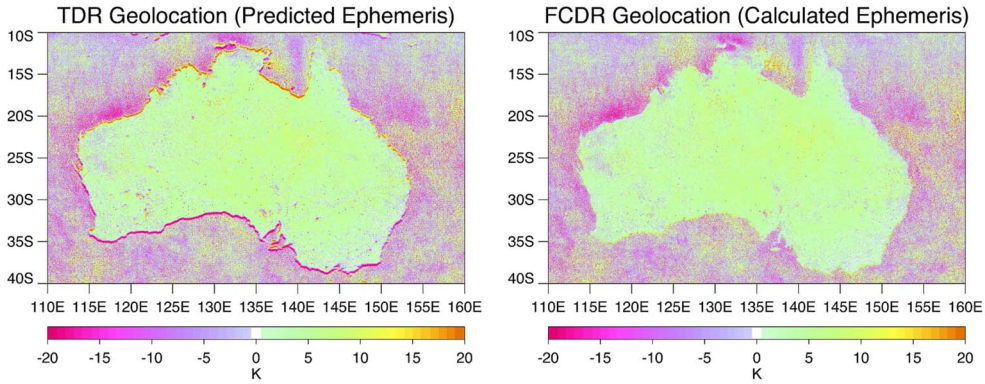

Fig. 4. Comparison of the F13 85-GHz horizontally polarized ascending minus descending Tb gridded at 1/20th of a degree for the 3-month period from April–June 1996. Results are shown for (a) original TDR pixel geolocation versus (b) FCDR calculated geolocation after applying the estimated roll, pitch, and yaw offsets.

There is no information available regarding deviations in the attitude of the DMSP spacecraft from nominal beyond the fixed values estimated by Colton and Poe's [2] coastline analysis, which is a significant issue for accurately calculating the EIA. Therefore, a full geolocation analysis of all of the SSM/I sensors is performed and described in the following sections.

II. Automated Method for Geolocation Analysis

An approach based on minimizing differences in mean Tb between ascending and descending swaths is used to examine differences in spacecraft attitude between the sensors as well as changes over time [11], [12]. Because land surfaces have substantially higher surface emissivity values than oceans, as shown in Fig. 1(a), window-channel radiometers such as SSM/I will show an apparent shift in the observed coastline, which is in opposite directions between the ascending and descending scans. By separately creating high-resolution grids of the ascending and descending scans over a period of a month or more and then differencing these, one is left with an image highlighting the coastline shift, as shown in Fig. 4(a). Note that a grid resolution higher than the spatial resolution of the sensor can be used, in this case 1/20th of a degree or ∼5 km, to identify subpixel geolocation errors. In that case, each pixel value is registered to the nearest grid box to the center of the pixel position, and sufficient sampling is required to at least fully populate all grid boxes.

The root-mean-square error (RMSE) of the temperature differences in the gridded difference map is used as a metric to determine the extent of the offset in the coastline. We chose the Australian coastline for the analysis as it provides large sections of coast oriented both east–west and north–south with lots of clear sky scenes, thus limiting the impact of weather events on the RMSE. Note that differences between the mean ascending and descending Tb maps due to the motion of large weather systems does not significantly change as the pixel geolocation is adjusted, although frequent weather over the coast will tend to mask the RMSE signal associated with the coastline shift. It is also important to have a scene with sufficient coast oriented in different directions to be able to independently distinguish the impact of offsets in the roll, pitch, and yaw. Fig. 4(b) shows the difference map based on the final pixel geolocation computed using the estimated roll, pitch, and yaw offsets. While the meteorological features remain, the outline of the coasts has disappeared.

Unfortunately, a significant limitation of this approach is the difficulty in distinguishing between the effects of changes in roll and yaw. For polar orbiting satellites aligned in a north–south direction, changes in roll and yaw have a similar signature with both affecting the geolocation by shifting the pixel geolocation in the east–west direction. As a result, an error in the estimate of the roll can be offset by a yaw error; therefore, simultaneous derivation of roll and yaw can be inaccurate. An independent technique was therefore developed to estimate roll based on the slope in the mean Tb across the scan. This

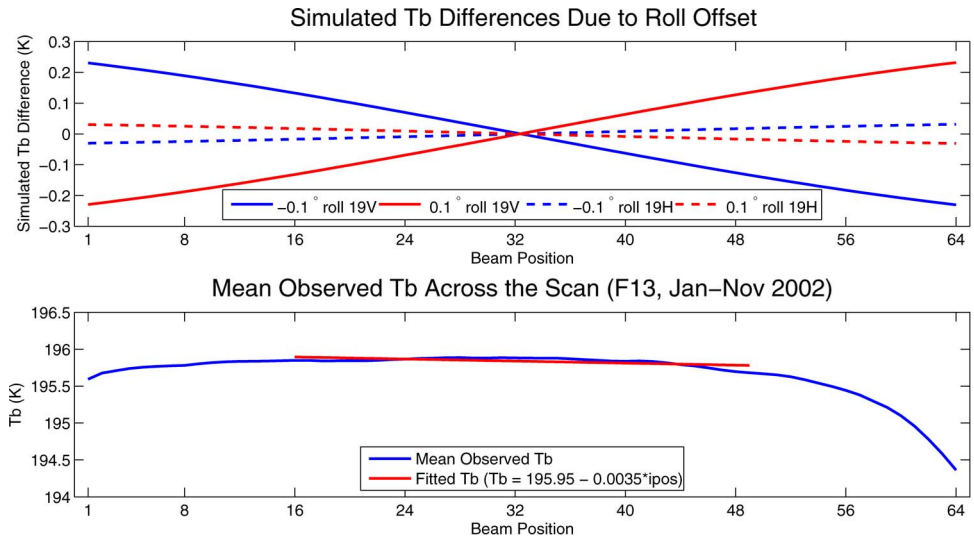

Fig. 5. Variations in Tb across the scan associated with an offset in the satellite roll. The top panel shows the simulated differences for roll offsets of -0.1 and 0.1 on both the 19v and 19h channels. The lower panel shows the observed mean Tbs across the scan from F13 over the period from January to November 2002 along with a linear fit to the center of the scan, which corresponds to a roll offset of -0.05.

technique exploits the fact that pitch and roll each have a very distinct effect on the Tb: Changes in pitch result in a symmetric curvature across the scan, whereas changes in roll result in a straight-line gradient across the scan. Yaw does not have an effect on the across-scan Tb for conical scanners. The simulated impacts of an offset in the roll are shown for the 19v and 19h channels in Fig. 5(a). As indicated in the figure, there is significantly less sensitivity in the 19h channel to changes in roll, and the changes in Tb are of the opposite sign to the 19v. Because of the smaller sensitivity of the horizontally polarized channels, only data from the vertically polarized channels were used. Fig. 5(b) shows the observed 19v Tb as a function of beam position averaged over an 11-month period of data. The data have been screened to eliminate land, sea ice, and rainfall. Since there is a well-known fall-off in energy at the right edge of the scan and, to a lesser extent, on the left side, the slope across the scan is computed via linear regression using only the middle 50% of the scan. The final linear fit is also shown in Fig. 5(b). Simulated results such as those shown in Fig. 5(a) are then used to translate the slope estimate into an estimate of the roll offset, which, in this case, gives an estimate of the roll offset of -0.05°. Roll estimates are independently computed for the 19v and 37v channels and then averaged together. The 85v and 22v channels are checked for consistency but are not used due to the failure of the 85v on F08 and the large biases in the 22v channel due to the operation of the radar calibration beacons on F15 after August 2006 [13]. Estimates of the roll are then used as inputs to the second step, which is to estimate pitch and yaw using the coastline analysis technique.

An automated minimization technique was developed to find the optimal pitch and yaw offsets based on minimizing the RMSE in the gridded ascending minus descending maps. The pixel geolocation was computed based on the known geometry of the sensor orientation, including sensor mount offsets; adjustments for roll, pitch, and yaw offsets to the spacecraft attitude; and spacecraft position and velocity calculated using two-line element (TLE) data and the North American Aerospace Defense Command SGDP4 code. It should be noted that calculating the spacecraft ephemeris based on the TLE files provides a more accurate estimate of the spacecraft position and velocity than the predicted ephemeris values that are stored with the original TDR data [9]. A fast optimization procedure was developed to estimate the pitch and yaw offsets that minimized the RMSE of the ascending minus descending grids for the specified roll value.

There is a tradeoff between temporal and spatial resolution or the length of time over which the ascending minus descending grid is aggregated versus the spatial resolution of the grid. To capture subtle shifts in the coastline between the ascending and descending passes and thus maximize the accuracy of the resulting pitch and yaw estimates, a high-resolution grid is required. Completely filling in the grid at a high spatial resolution, however, requires a large amount of data. Using the high-resolution 85-GHz horizontally polarized Tb data, a grid resolution of 1/20th of a degree was chosen, which roughly translates to around 5 km or an approximately 0.1° pitch offset. Although a three-month data window was found to adequately populate the grid, an 11-month moving window was ultimately used in order to smooth out the results and to minimize the effect of both noise due to sampling and weather, as well as short-term or spurious changes. This does eliminate the possibility of capturing short-term seasonal or subseasonal changes in the spacecraft attitude; however, the goal of this analysis is to identify long-term changes in the spacecraft attitude for climate applications. As a result, the tradeoff in favor of high accuracy (i.e., high spatial grid resolution) was chosen at the expense of relatively low temporal resolution.

III. Results

Roll estimates are shown over the life of each of the six sensors in Fig. 6(a) based on the approach using the slope of the mean Tb across the scan, as described earlier. Although there are differences between the sensors, in general, the calculated

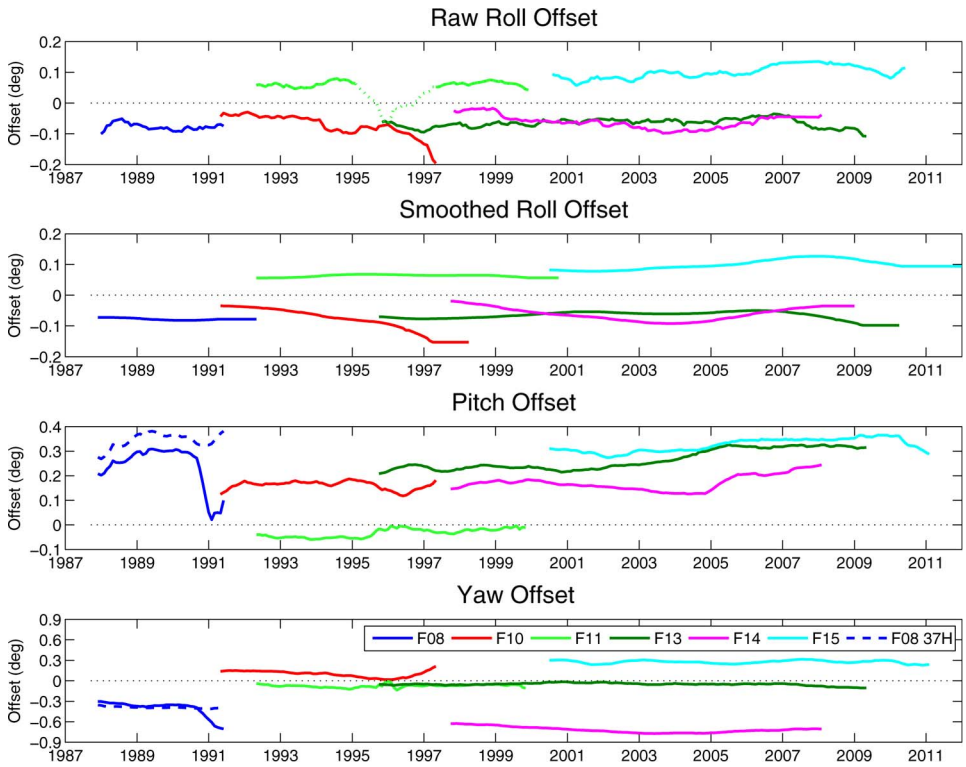

Fig. 6. Comparison of the time series of the original (raw) and smoothed estimates of roll, and the original estimates of the pitch and yaw offsets for F13. All of the values were computed using an 11-month running mean data window.

roll offset values are very consistent over the lifetime of each satellite/sensor. There are, however, a couple of exceptions to this, including a significant decrease in the roll offset for F10 toward the end of its life and an anomalous decrease in the roll estimates for F11 in late 1995. Although not fully understood, the change in the roll offset toward the end of the F10 lifetime appears to be real. The decrease in the F11 roll offset in late 1995, however, was determined to be not due to the effect of roll since its magnitude is as large in the horizontally polarized channels as in the vertically polarized channels, despite the former being less sensitive to changes in the view angle and, thus, roll [see Fig. 5(a)]. While it is not clear what is causing this anomalous change in mean Tb across the scan, since it does not appear related to a spacecraft roll, the values for this period were removed and interpolated using a smoothing spline. The dotted line in Fig. 6(a) indicates the period of anomalous roll estimates for F11 that were removed and interpolated across for the final roll estimates. A smoothing spline is subsequently applied to the time series of calculated roll offset values to create the final roll values shown in Fig. 6(b). These smoothed estimates of the roll offsets are then used as input into the coastline analysis procedure used to compute estimates of the pitch and yaw offsets.

Time series of the computed pitch and yaw adjustments over the life of each of the six SSM/I sensors are shown in Fig. 6(c) and (d). With a few notable exceptions, the attitude for each spacecraft is relatively consistent over time, although differences between the satellites are significant. One exception is the dramatic decrease in the pitch offset for F08. This is due to the failure of the 85h channel in February 1991. Due to the 11-month time window used, the pitch and yaw estimates start to change in late 1990. To account for the failure in the 85h channel, the coastline analysis was redone using the 37v channel. The resulting pitch and yaw offsets from F08 using the 37h channel are shown by the dashed blue lines in Fig. 6(c) and (d). While there are slight differences, the pitch and yaw estimates from the 37h analysis show no abrupt fall-off. As a result, the values from the 37h analysis prior to mid-1990 are bias adjusted to the values from the 85h analysis and then used over the full data record. As with the roll estimates, the monthly pitch and yaw estimates are subsequently smoothed using a spline interpolation to further reduce/eliminate high-frequency variability and/or noise.

The final smoothed values of roll, pitch, and yaw are shown in Fig. 7. The range of the roll offsets is smaller than the associated pitch and yaw adjustments with values generally within $\pm 0.1^{\circ}$. This is expected and is consistent with previous results [2], [9]; however, it does not imply less accuracy in the pitch and yaw estimates. While the time-dependent changes are generally small, differences between sensors are significant. It should be noted that the changes over time as well as the differences in the roll, pitch, and yaw offsets between sensors are likely the result of error sources in addition to changes in the attitude of the spacecraft. The roll, pitch, and yaw offsets computed here should therefore be considered as somewhat generic corrections to adjust for pixel geolocation errors resulting from a combination of potential error sources. Poe and Conway [9] provide a list of candidate error sources that include: 1) spacecraft orbital elements; 2) predict spacecraft ephemeris data; 3) sensor pixel location algorithm;

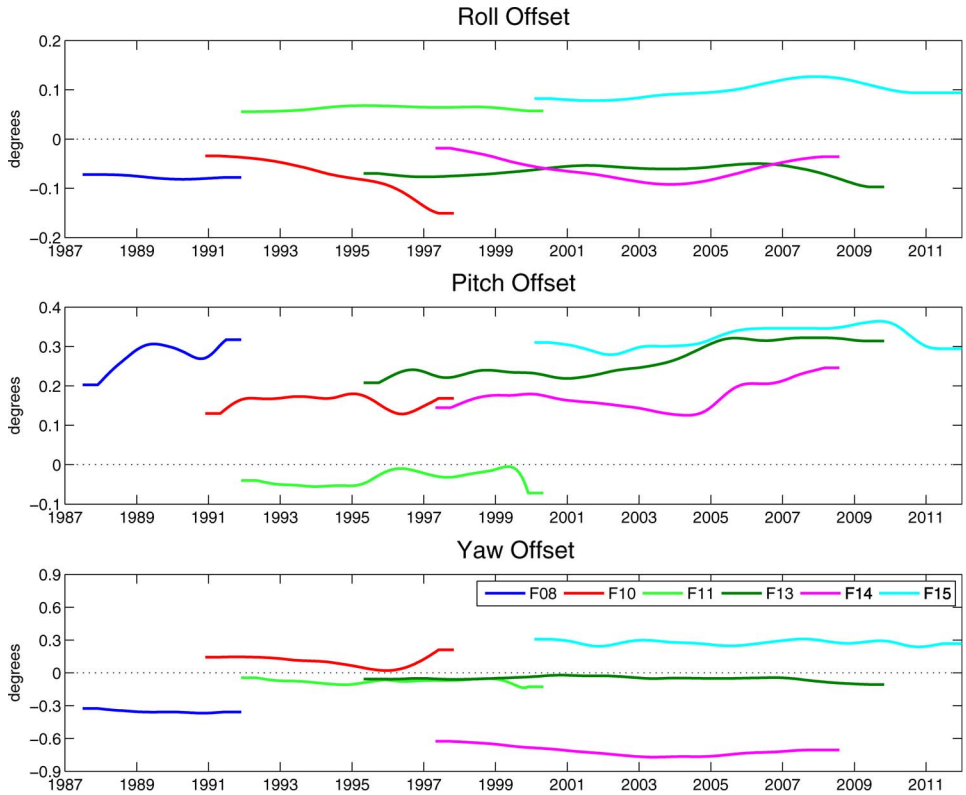

Fig. 7. Time series of the final roll, pitch, and yaw offsets for each of the SSM/I sensors calculated based on the geolocation analysis. The values are based on an 11-month running mean and have been further smoothed to remove random variations and high frequency variability.

4) sensor deployment/alignment of spin axis; 5) sensor alignment to spacecraft; and 6) spacecraft attitude. They note that the misalignment of the sensor to the spacecraft is reported to be not greater than 0.1° and the deployment errors are less than 0.03°. The primary spacecraft attitude control system uses gyro signals as a short-term reference, star mapper inputs for updates, and a stored ephemeris table to relate the inertial attitude to the desired Earth-pointing direction. There is also a backup system to check the Earth pointing to an overall accuracy value of within 0.12°. Unfortunately, it is not possible to verify or even to determine the accuracy of most of these component issues, although the magnitude of the results shown here is not inconsistent with those from Poe and Conway [9] or with the magnitude of geolocation errors found with other conically scanning radiometers such as the Special Sensor Microwave Imager Sounder, WindSat, and Advanced Microwave Scanning Radiometer-EOS [11], [14], [15].

The impact of changes in roll, pitch, and yaw on EIA is somewhat complicated. A change in pitch of 1° results in a $\sim 1.3^\circ$ change in the EIA at the center of the scan and a $\sim 0.8^\circ$ change in EIA at the edge of the scan. A 1° change in the roll results in a $\sim 1.0^\circ$ increase in the EIA at the edge of the scan and no change in EIA at the center of the scan. Changes in yaw have no impact on EIA, although it does impact the geolocation. Thus, the differences in pitch between the satellites shown in Fig. 7 of several tenths of a degree will translate to comparable differences in EIA, which in turn can lead to Tb differences of up to 0.5 K. Similarly, the changes in pitch over time can introduce a small but significant time-dependent bias in the Tb if not properly accounted for.

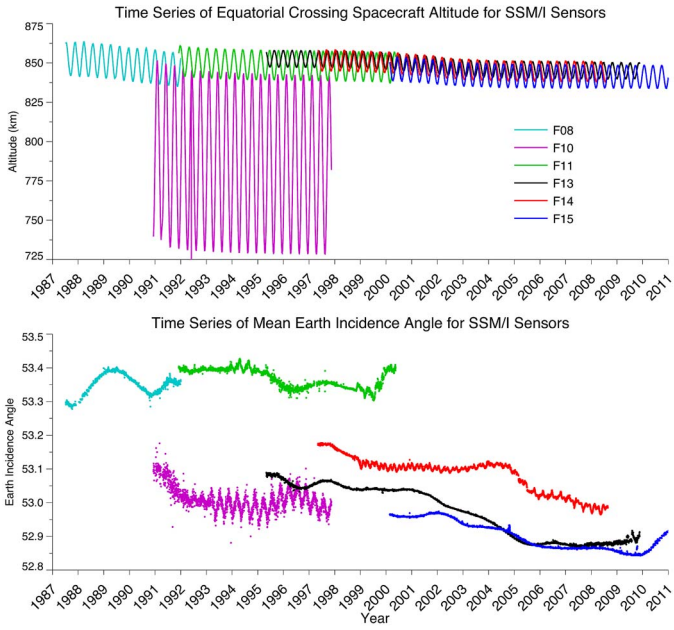

Fig. 8. Time series for each of the six SSM/I sensors of (a) altitude of the spacecraft at the equator for the ascending part of the orbit and (b) mean EIA.

Fig. 8 shows changes in time in the spacecraft altitude at the equatorial crossing point for the ascending part of the orbit, as well as the mean EIA for each of the six sensors. Because there is no active control system on the DMSP spacecraft to maintain the orbit, the altitude decreases over time for each of the satellites. There is also a periodic change as the orbits

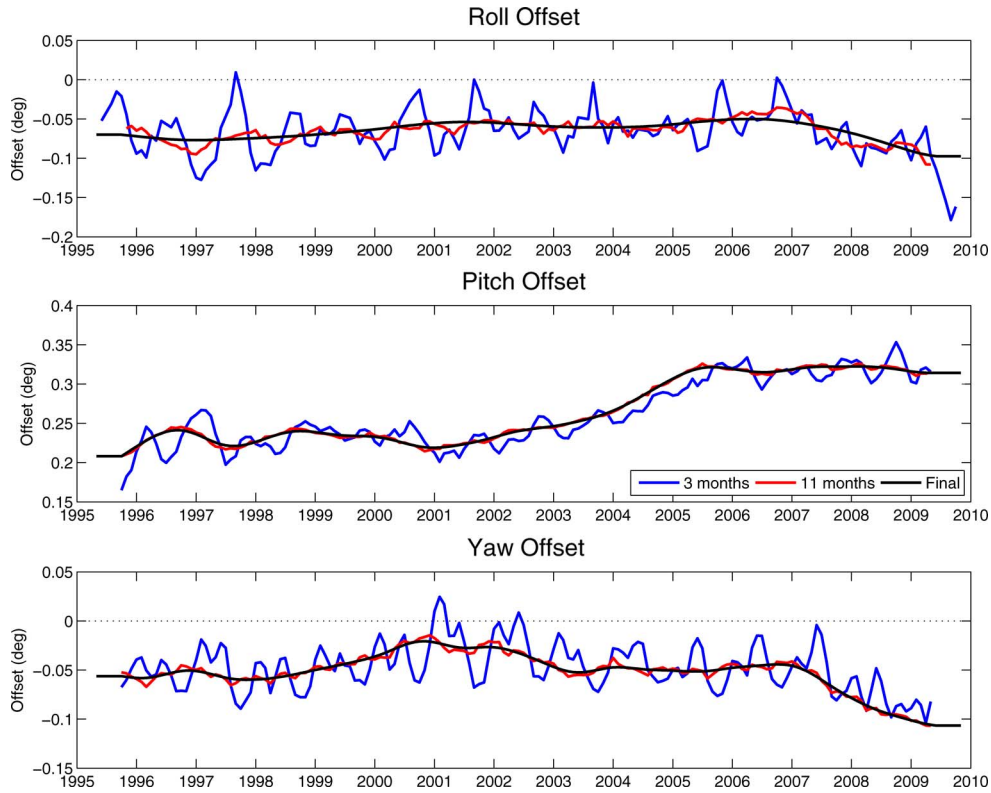

Fig. 9. Comparison of the ime series of the calculated roll, pitch, and yaw offsets for F13 computed using a 3-month versus 11-month running mean. The black line shows the final smoothed values.

are slightly elliptical and the orbits precess over time. F10 in particular is in a much more elliptical orbit with a lower mean altitude. The EIA variations shown in Fig. 8(b) indicate a significant decrease over time for each of the sensors resulting from the decrease in altitude. This time-dependent change in EIA due to the altitude decrease is typically much more significant than the time-dependent changes in the spacecraft attitude shown in Fig. 7. Although these changes are small, they are not insignificant relative to some climate signals. It is important to note, therefore, that geophysical retrieval algorithms that do not properly account for these changes in the EIA could produce artificial climate trends or mask real physical climate signals.

IV. Uncertainties in the Spacecraft Attitude Estimates

As aforementioned, data from the 85-GHz horizontally polarized channel was used to create ascending and descending Tb grids with a spatial resolution of 1/20th degree and accumulated over a time window of 11 months. Since the analysis was done for each month using a moving data window, we chose in this case to use a data window of ± 5 months for a total data window of 11 months. Fig. 9 shows a comparison of the roll, pitch, and yaw estimates for F13 using 3-month and 11-month time windows, as well as the final spline smoothed results. As Fig. 9 shows, the resulting roll and yaw estimates appear somewhat noisier than the pitch estimates. Given that pitch offset impacts the EIA more than the roll, with the exception of the very edge of the scan, and the yaw does not affect the EIA at all, the residual errors in the calculated EIA are primarily due to errors in the estimated pitch offset. The pitch estimates in Fig. 9 based on a 3-month time window show significant variability due to either limited sampling or seasonal variations in the pitch; however, the amplitude of this "noise" is still within 0.05°. Using an 11-month time window significantly decreases this variability, and it is eliminated by subsequently smoothing the time series. Of course, this means that potential seasonal variability in the spacecraft attitude is removed; however, the amplitude of these variations is typically less than 0.05°, which is of similar magnitiude to other potential sources of error.

Fig. 10 shows pitch and yaw differences based on an independent analysis of each of the seven SSM/I channels. Since the spatial resolution of the 19-, 22-, and 37-GHz channels is half that of the 85-GHz channel, a grid resolution of 1/10th of a degree was used in order to adequately populate the grids. The results for all channels are based on an 11-month time window and have been subsequently smoothed. Results based on grid resolutions of both 1/10th and 1/20th of a degree are shown for the 85-GHz H-pol channel to show the impact of spatial resolution on the results. Although all seven SSM/I channels share the same feedhorn, it is possible that they can have slightly different focal points due to the electronics, thus leading to slight differences in the pointing. This comparison also provides a consistency check for the technique as the impact of meteorology and the land/ocean contrast differs somewhat between channels. While there are differences in the

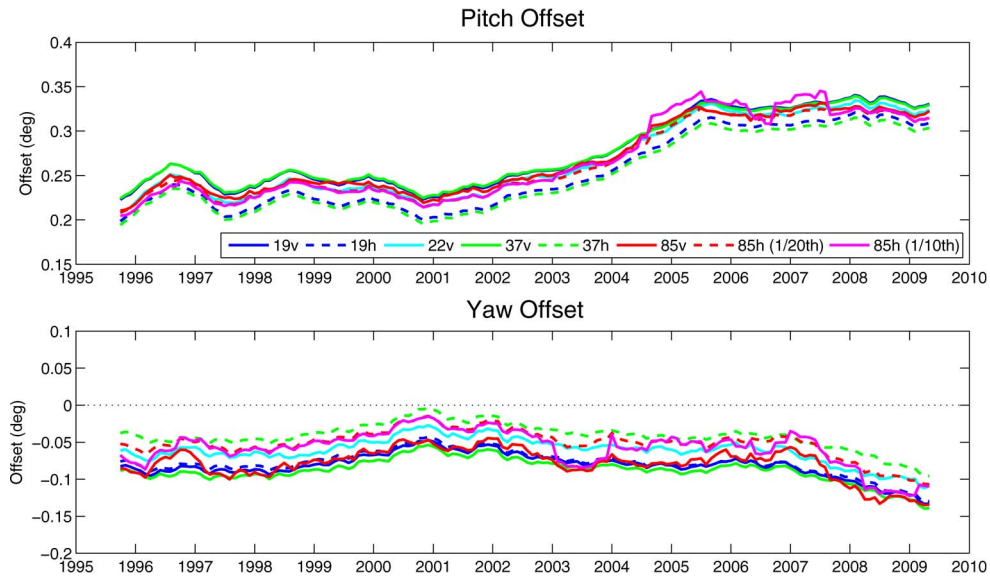

Fig. 10. Time series of the calculated pitch and yaw offsets for F13 computed independently for each of the seven channels. In addition, the pitch and yaw estimates were computed for the 85h channel using both a 1/10th and 1/20th of a degree grid resolution.

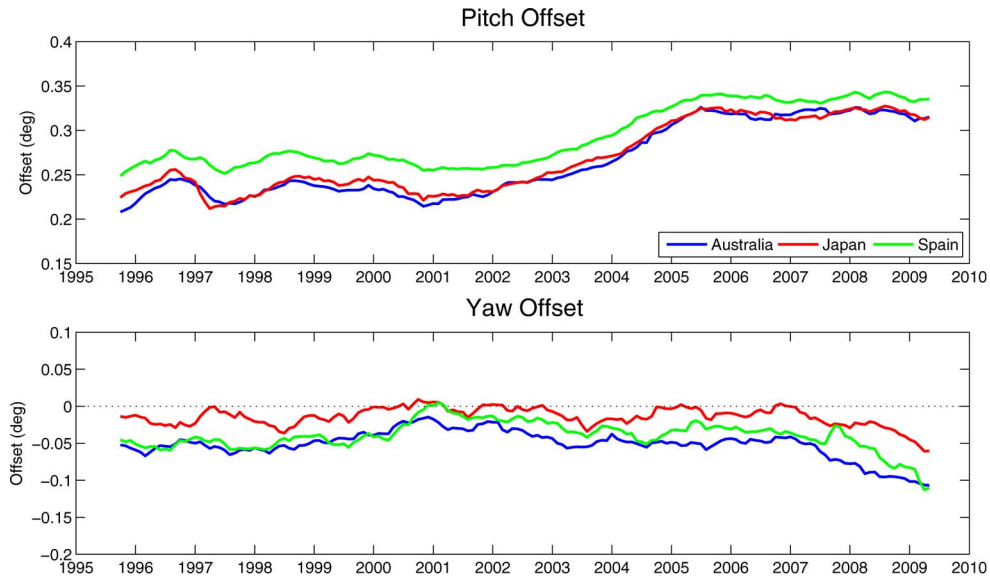

Fig. 11. Comparison of time series of the calculated pitch and yaw offsets for F13 computed from three different regions including Australia, Spain, and Japan.

pitch adjustments for the seven channels, the differences are all within $\sim 0.05^{\circ}$.

A final comparison of the estimated pitch and yaw values from F13 was done using three different regions, including Australia, Japan, and Spain. These regions all have significant coastlines oriented in both east–west and north–south directions and are also over very different geographical regions both in latitude and longitude. The results shown in Fig. 11 indicate some differences, but both the pitch and yaw estimates are once again within $\sim 0.05^{\circ}$. As noted previously, the primary attitude control system for the DMSP spacecraft uses a star tracker; therefore, the reason for these regional differences is not clear, although they are small enough to be effectively ignored. In summary, modifications to the grid resolution, time window, channel selection, and region used all show robust estimates of roll, pitch, and yaw within 0.1°. Although uncertainties in the roll and yaw estimates are somewhat larger, particularly in terms of the higher frequency changes shown in Fig. 9, they are also within 0.1°. For all six sensors, the long-term changes are quite stable indicating that the computed EIA is generally accurate to within 0.1°.

A subsequent analysis of gridded ascending minus descending images for each month, similar to that shown Fig. 4, was done over the life of each of the six sensors. While an animation of these images (not shown) shows some small changes, the presence of visible coastline offsets is greatly reduced in all cases, giving a high degree of confidence that the final computed geolocation and EIA estimates are a significant improvement from the original geolocation. The conclusion that the long-term changes in EIA are accurate to within 0.1°

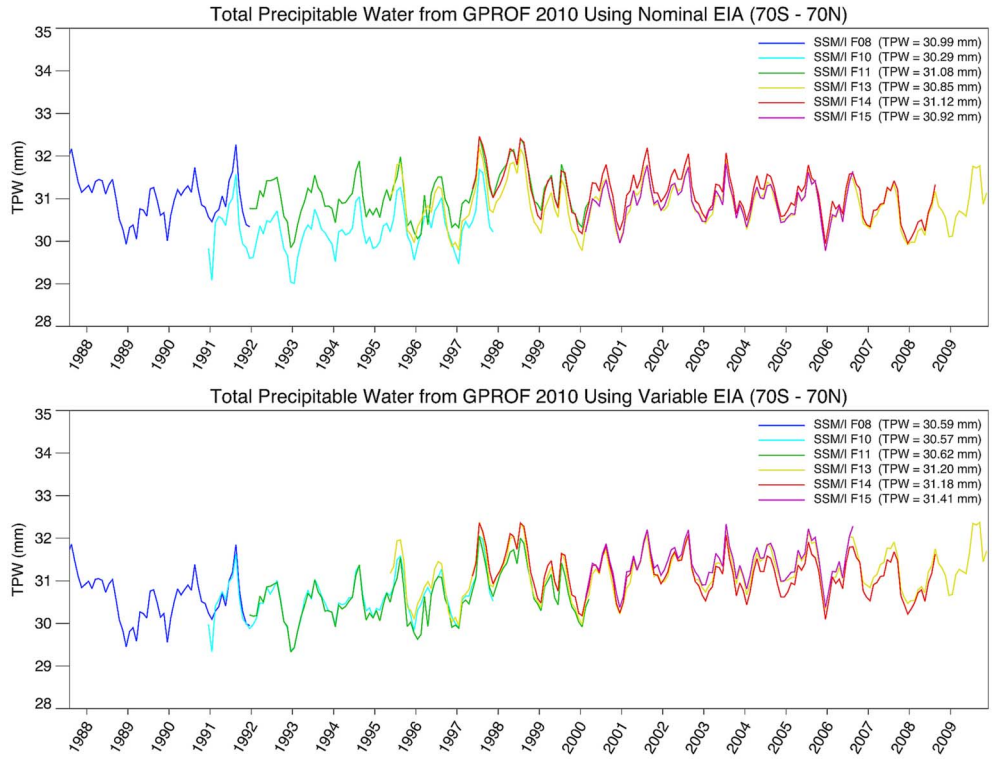

Fig. 12. Time series of TPW from the GPROF 2010 retrieval algorithm from the series of six SSM/I sensors using (a) nominal EIA values and (b) the variable EIA values computed based on the geolocation analysis.

also means that, in terms of the view-angle impact, residual differences in the intercalibration, as shown in Fig. 3, should be within 0.2 K for the vertically polarized channels and within 0.1 K for the horizontally polarized channels.

V. Summary

An analysis of changes in spacecraft attitude over time has been performed over the period from July 1987 through December 2009 for all six of the SSM/I sensors, which operated on board DMSP F08, F10, F11, F13, F14, and F15. Estimates of the roll, pitch, and yaw offsets were computed and applied to the data. The results were generally quite stable over time, with some variations in the F08 and F10 records as well as slowly varying increases in the F13 pitch over time. An analysis of uncertainties in the estimates was subsequently performed by varying different aspects of the analysis, including the spatial resolution of the grid, the temporal resolution or data time window, the region analyzed, and the channel used. In all cases, the resulting differences were within $\sim 0.05^\circ$ for the pitch and within 0.1° for the roll and yaw. This translates to an error of less than 0.1° in mean EIA and less than 5 km in the geolocation. While there is some evidence pointing to higher frequency variations in spacecraft attitude in some cases, a visual analysis of the residual geolocation errors over monthly scales shows a substantial improvement over the original pixel geolocation and generally very stable results over time.

While the improvement to the pixel geolocation to within ~ 5 km is useful, for most applications, it will have little impact. Improvements to the calculated values of the EIA for each pixel over the nominal published values, however, can have a significant impact for both the intercalibration of the sensors as well as for creating CDRs of variables such as TPW, ocean surface winds, and precipitation. Differences in both the altitude and attitude of each of the sensors as well as decreases in the altitude over time lead to time-dependent changes in EIA and significant differences between the sensors. The mean differences in EIA between sensors, which are as much as 0.5°, can lead to differences in the vertically polarized Tb of up to 1 K. Using the computed EIA values based on this analysis, however, reduces potential biases in the intercalibration to less than 0.2 K for the vertically polarized channels and below 0.1 K for the horizontally polarized channels. Therefore, this is a critical first step before performing any intercalibration of the sensors. It is also important that algorithm developers that use the intercalibrated FCDR data to create TCDRs use the computed EIA values to properly account for differences in the observed Tb that are due to changes in view angle.

Fig. 12 shows an example of changes in a long-term record of TPW from each of the six SSM/I sensors between using nominal values of EIA (top panel) versus the computed EIA values (bottom panel). It should be noted that intercalibration offsets were applied to the input data for both time series. The TPW estimates shown here are from the OE approach developed in [10] and implemented as part of the Goddard Profiling (GPROF) rainfall retrieval algorithm used operationally to produce rainfall retrieval for the Tropical Rainfall Measuring Mission and AMSR-E [16], [17]. While this retrieval algorithm has not been validated using *in situ* observations and is thus not suitable for climate analysis, it does account for changes in EIA and is thus useful for investigating the impact of changes in EIA on TPW estimates. The impact of EIA is most evident

in the retrieval from F10, which, as shown in Fig. 8(a), is in a much more elliptical orbit, but generally, the consistency between sensors is greatly improved when properly accounting for EIA differences. Residual differences due to different local observing times between the sensors and, thus, real diurnal differences remain as well as other potential issues, but this example demonstrates that differences in EIA cannot be ignored by TCDR developers.

ACKNOWLEDGMENT

The authors would like to thank S. Bilanow at NASA's Goddard Space Flight Center for his invaluable assistance in coding and verifying the pixel geolocation code used in this analysis.

REFERENCES

[1] J. P. Hollinger, J. L. Pierce, and G. A. Poe, "SSM/I instrument evaluation," *IEEE Trans. Geosci. Remote Sens.*, vol. 28, no. 5, pp. 781–790, Sep. 1990.

[2] M. C. Colton and G. A. Poe, "Intersensor calibration of DMSP SSM/I's: F-8 to F-14, 1987–1997," *IEEE Trans. Geosci. Remote Sens.*, vol. 37, no. 1, pp. 418–439, Jan. 1999.

[3] NRC, *Climate Data Records from Environmental Satellites*. Washington, DC: National Academy Press, 2004.

[4] F. J. Wentz, "A well-calibrated ocean algorithm for Special Sensor Microwave/Imager," *J. Geophys. Res.*, vol. 102, no. C4, pp. 8703–8718, Apr. 1997.

[5] S. T. Brown and C. S. Ruf, "Determination of an amazon hot reference target for the on-orbit calibration of microwave radiometers," *J. Atmos. Ocean. Technol.*, vol. 22, no. 9, pp. 1340–1352, Sep. 2005.

[6] S. Brown, S. Desai, S. Keihm, and W. Lu, "Microwave radiometer calibration on decadal time scales using on-earth brightness temperature references: Application to the TOPEX microwave radiometer," *J. Atmos. Ocean. Technol.*, vol. 26, no. 12, pp. 2579–2591, Dec. 2009.

[7] A. Andersson, K. Fennig, C. Klepp, S. Bakan, H. Gral, and J. Schulz, "The Hamburg ocean atmosphere parameters and fluxes from satellite data—HOAPS-3," *Earth Syst. Sci. Data*, vol. 2, no. 2, pp. 215–234, Sep. 2010.

[8] S. Yang, F. Weng, B. Yan, N. Sun, and M. Goldberg, "Special Sensor Microwave Imager (SSM/I) intersensor calibration using a simultaneous conical overpass technique," *J. Appl. Meteorol. Climatol.*, vol. 50, no. 1, pp. 77–95, Jan. 2011.

[9] G. A. Poe and R. W. Conway, "A study of the geolocation errors of the Special Sensor Microwave/Imager (SSM/I)," *IEEE Trans. Geosci. Remote Sens.*, vol. 28, no. 5, pp. 791–799, Sep. 1990.

[10] G. S. Elsaesser and C. D. Kummerow, "Toward a fully parametric retrieval of the nonraining parameters over the global oceans," *J. Appl. Meteorol. Climatol.*, vol. 47, no. 6, pp. 1599–1618, Jun. 2008.

[11] H. Wiebe, G. Heygster, and L. Meyer-Lerbs, "Geolocation of AMSR-E data," *IEEE Trans. Geosci. Remote Sens.*, vol. 46, no. 10, pp. 3098–3103, Oct. 2008.

[12] G. Heygster, H. Wiebe, G. Spreen, and L. Kaleschke, "AMSR-E geolocation and validation of sea ice concentrations based on 89 GHz data," *J. Remote Sens. Soc. Jpn.*, vol. 29, no. 1, pp. 226–235, Jan. 2009.

[13] K. A. Hilburn and F. J. Wentz, "Mitigating the impact of RADCAL beacon contamination on F15 SSM/I ocean retrievals," *Geophys. Res. Lett.*, vol. 35, pp. L18806-1–L18806-3, Sep. 2008.

[14] G. A. Poe, E. A. Uliana, B. A. Gardiner, T. E. von Rentzell, and D. B. Kunkee, "Geolocation error analysis of the Special Sensor Microwave Imager/Sounder," *IEEE Trans. Geosci. Remote Sens.*, vol. 46, no. 4, pp. 913–922, Apr. 2008.

[15] W. E. Purdy, P. W. Gaiser, G. A. Poe, E. A. Uliana, T. Meisner, and F. J. Wentz, "Geolocation and pointing accuracy analysis for the windsat sensor," *IEEE Trans. Geosci. Remote Sens.*, vol. 44, no. 3, pp. 496–505, Mar. 2006.

[16] C. Kummerow, Y. Hong, W. S. Olson, S. Yang, R. F. Adler, J. McCollum, R. Ferraro, G. Petty, D.-B. Shin, and T. T. Wilheit, "The evolution of the Goddard profiling algorithm (GPROF) for rainfall estimation from passive microwave sensors," *J. Appl. Meteorol.*, vol. 40, no. 11, pp. 1801–1820, Nov. 2001.

[17] C. D. Kummerow, S. Ringerud, J. Crook, D. Randel, and W. Berg, "An observationally generated a priori database for microwave rainfall retrievals," *J. Atmos. Ocean. Technol.*, vol. 28, no. 2, pp. 113–130, Feb. 2011.

Wesley Berg received the B.S., M.S., and Ph.D. degrees from the University of Colorado, Denver, in 1988, 1989, and 1993, respectively, all in aerospace engineering.

He was previously with the Cooperative Institute for Research in Environmental Science, Environmental Research Laboratories, NOAA. He is currently a Senior Research Scientist with the Department of Atmospheric Science, Colorado State University, Fort Collins. His research interests include satellite remote sensing of precipitation and other hydrologic parameters with a focus on the development and analysis of satellite retrieval for climate applications.

Mathew R. P. Sapiano received the B.Sc. and M.Sc. degrees in statistics and the Ph.D. degree in meteorology from the University of Reading, Reading, U.K., in 2000, 2001, and 2005, respectively.

From 2009 to 2012, he was a Research Scientist with the Department of Atmospheric Science, Colorado State University, Fort Collins. Since 2012, he has been an Assistant Research Scientist with the Earth Systems Science Interdisciplinary Center, University of Maryland, College Park.

Jennifer Horsman received the A.B. degree in geophysics from the University of California at Berkeley, Berkeley, in 1993 and the M.S. degree in environmental science and policy from Plymouth State University, Plymouth, NH, in 2008.

She is currently a Computer Systems Engineer with the Visualization Group, Lawrence Berkeley National Laboratory, Berkeley, CA. Her research interests include scientific data visualization, geographic information systems, glacial geology, and applied geophysics.

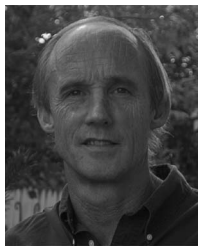

Christian Kummerow received the A.B. degree in physics from the University of California at Berkeley, Berkeley, in 1982 and the Ph.D. degree in atmospheric physics from the University of Minnesota, Minneapolis, in 1987.

Between 1997 and 2000, he served as a Project Scientist for the Tropical Rainfall Measuring Mission. He is currently a Professor with the Department of Atmospheric Science and the Director of the Cooperative Institute for Research in the Atmosphere, Colorado State University, Fort Collins. His research interests include rainfall and its variability in the climate system. He has developed rainfall products from passive microwave sensors and combined active/passive methods. Understanding uncertainties in these estimates forms the basis of climate studies that seek to understand the sensitivity of precipitation to increased greenhouse gas concentrations. Significant research is therefore focused on precipitation as part of the climate System with efforts focused on closing the water and energy budgets over not only at global but also at regional scales.

Dr. Kummerow is currently the Chair of the GEWEX Data and Assessments Panel.